Precoded Single-Cell Multi-User MISO Visible Light Communications

Precoded Single-Cell Multi-User MISO Visible Light Communications

Tezcan Cogalan*, Harald Haas* and Erdal Panayirci†

*Institute for Digital Communications
Li-Fi Research and Development Centre
The University of Edinburgh
Edinburgh, EH9 3JL, UK
Email: {t.cogalan, h.haas}@ed.ac.uk

†Kadir Has University
Department of Electronics Engineering
Istanbul, 34083, Turkey
Email: {eepanay}@khas.edu.tr

***Abstract*—This study investigates the effects of transmitter and receiver parameters on the performance of a precoded, single-cell (SC), multi-user (MU), multi-input-single-output (MISO) visible light communication (VLC) system. A zero-forcing (ZF) precoding technique is used within the constraints of optical transmission power and non-negativity of an intensity modulated (IM) transmitted signal. The simulation results show that the physical features of the light emitting diode (LED) and photodiode (PD) have a significant effect on the bit error rate (BER) and total spectral efficiency (SE) performance of the VLC system. The deployment with 8 users and 45° receiver field-of-view (FOV) achieves both the targeted BER and approximately 50 bits/s/Hz total SE when the transmitter semi-angles are 30° and 60°.**

I. Introduction

With the enhanced capability of electronic devices, mobile devices and their applications are becoming smarter. Inherently, popularity of these smart devices is increasing. Therefore, demand for wireless data is increasing and it is expected to exceed 15 exabytes by 2018 [1]. Due to demand for high speed wireless data in various environments, service providers have had to deploy more, even smaller cells. Hence, the capacity of the radio frequency (RF) spectrum has almost reached its limit and the frequency spectrum beyond the RF spectrum has been explored to transfer the RF spectrum burden [2, 3].

One of the proposed solutions to the RF spectrum crisis is visible light communications (VLC) [3]. VLC technology uses widely available white light emitting diodes (LEDs) for signal transmission using intensity modulation (IM), and photodiodes (PDs) for signal receiving using direct detection (DD) techniques, and operates in the 400–490 THz frequency range [4]. Using the existing lighting infrastructure and low cost transmitter-receiver components, VLC is a candidate technique for small cell deployments to complement RF indoor communications [3].

Using the widely available LEDs and recent developments in power efficient CMOS design, multiple input single output (MISO) and multiple input multiple output (MIMO) techniques have improved the performance of the VLC technology [4–6]. However, interference is becoming a system limiting factor of densely deployed cellular systems. Therefore, interference mitigation techniques such as precoding, and different access and modulation types have a primary importance on the system performance.

In the RF wireless communication systems, the precoding technique has been extensively researched. However, precoding techniques have recently been studied in indoor optical MISO and MIMO wireless communications [7–10]. VLC has some differences from RF based communications. On the one hand, transmitted signal and channel coefficients are real valued and positive in VLC. On the other hand, transmitted signal and channel coefficients may have complex and positive or negative values in RF communications. Based on these VLC characteristics, conventional RF precoding techniques cannot be applied directly [8, 10]. The non-negativity of the IM signal and non-linearity effect of an LED should be considered in the precoder design for the VLC [10].

In published research, a single-user optical MIMO system has been studied using different precoder schemes [7, 8]. In [8], a free space optical (FSO) channel is considered corresponding to Rayleigh and lognormal channel models in the system, and a singular value decomposition (SVD) based precoder design is used to satisfy the non-negativity of the IM signal with allocating optical power, offset value and modulation size. Also, in [7], the precoder is designed according to the non-negativity of the modulated signal using the SVD based design. Different from [8], in [7], a Lambertian radiant intensity model is used to generate the channel gains.

In addition to the single-user models, a multi-user MISO in VLC is studied when a zero-forcing (ZF) and a minimum mean square error (MMSE) based precoders are used, in [9] and [10] respectively. In both studies, convex programming tools are used to design the precoder. In [10], the non-negativity of the modulated signal and the linear region of the LED are considered as optimization problem constraints, and the MMSE technique is used as the performance metric to design the precoder.

In [9], the ZF and ZF-dirty paper coding (DPC) techniques are used to precode the user data. The precoders are designed according to the non-negativity and total optical power constraints. The performance of both precoders are compared when users are located close and far away from each other. While the ZF-DPC outperforms the ZF in theory, it is difficult to implement in practice due to its complexity [11].

ISBN 978-3-8007-3976-9

In this study, the ZF based linear precoding technique is used as designed in [9], when a single-cell with multiple LEDs and multi-users with single PD MISO system is deployed. Different from [9], one LED array with multiple LEDs is used as a transmitter in order to investigate the effects of the LED semi-angle and the field-of-view (FOV) of the PD on the system bit error rate (BER) which is averaged according to number of deployed users and on the total spectral efficiency (SE) performance which is a summation of the achieved SE of deployed users. Also, the system performance is obtained when different number of users are located randomly in an indoor environment.

It is important to note that the number of transmitters should be equal to or larger than the total number of receivers in the ZF precoding. In VLC, this is a constraint which can be managed due to the ease of deploying several LEDs in a small LED array [5].

The paper is organized as follows. The system model is described in Section II, including the signal transmission/reception and precoder designed under optical transmission constraints. The simulation parameters used and results are presented in Section III. Finally, conclusions are drawn in Section IV.

II. System Model

A single-cell multi-user optical wireless MISO system is considered. The system is equipped with a single LED array $(N_t = 1)$ which consists of multiple LEDs $(N_{t,\ell} = 1, 2, ..., L)$ at the transmitter side, and multiple users $(k = 1, 2, ..., K)$ with a single PD $(N_r = 1)$ at the receiver side. The received signal vector is shown by the conventional discrete model:

$$\mathbf{y} = r\mathbf{H}\mathbf{x} + \mathbf{n}, \tag{1}$$

where $\mathbf{y}$ is the $(K\text{x}1)$ received signal vector; r is the PD responsivity (optical-to-electrical conversion factor) constant; $\mathbf{H}$ is the $(K\text{x}L)$ channel DC gain matrix; $\mathbf{x}$ is the $(K\text{x}1)$ precoded transmit data vector; and $\mathbf{n}$ is the real-valued $(K\text{x}1)$ noise vector with zero-mean and σ_n^2 variance. In this study, both a thermal noise due to circuit components at the receiver side and an ambient shot light noise due to surrounding light sources are considered. Thus, the noise variance σ_n^2 is:

$$\sigma_n^2 = 2er\left(P_{signal,k} + P_{ambient,k}\right)B + i_{amp}^2 B, \tag{2}$$

where e is the electronic charge; $P_{signal,k}$ is the average received power at user k; B is the receiver bandwidth; and $P_{ambient,k}$ is the received ambient light power at user k:

$$P_{signal,k} = \mathbf{H}_k\mathbf{P}, \tag{3}$$

$$P_{ambient,k} = \chi_{amb}A_{R_x}2\pi\left(1 - \cos(\theta_k)\right), \tag{4}$$

where $\mathbf{H}_k$ is the $(1\text{x}L)$ channel DC gain vector for user k; $\mathbf{P}$ is the $(L\text{x}1)$ DC bias vector for the LED array; χ_{amb} is the photocurrent of the ambient light power; A_{R_x} is the physical area of the receiver; and θ_k is the incidence angle from the transmitter to receiver k.

A. Transmitter

In a VLC system, the IM is used at the transmitter side which modulates instantaneous optical power of the LED. Hence, the transmitted signal in the VLC system is a non-negative and real-valued signal. In this study, 2-pulse amplitude modulation (PAM) is used for signal shaping, and different DC bias power values, P_b, are used to move the symbol transmitted to user k, $s_k \in [-1, 1]$, to the linear region of the LED. In addition to that, the symbol for user k is coded by the ZF precoding scheme before adding the DC bias power. Thus, the transmitted signal $\mathbf{x}$ is:

$$\mathbf{x} = \mathbf{F}\mathbf{s} + \mathbf{P}, \tag{5}$$

where $\mathbf{F}$ is the $(L\text{x}K)$ ZF precoder matrix; $\mathbf{s}$ is the $(K\text{x}1)$ generated data vector for users; and $\mathbf{P}$ is the $(L\text{x}1)$ DC bias vector consists of bias power of each LED $P_{b,\ell}$:

$$\mathbf{P} = \left[P_{b,1}, ..., P_{b,\ell}, ..., P_{b,L}\right]^{\mathrm{T}}. \tag{6}$$

As noted, precoding techniques used in RF systems could not be directly implemented in the VLC systems. The non-negativity constraint of the transmitted signal and output optical power constraint of the LED should be considered in the precoder design. As shown in [9], the symbol transmitted from each LED should satisfy the given constraint:

$$\sum_{k=1}^{K} |f_{\ell,k}| <= P_{b,\ell}, \tag{7}$$

where $\mathbf{f}_\ell$ represents ℓ^{th} row of the precoder matrix $\mathbf{F}$. According to the conventional ZF beamforming [12], multiplication of the precoder matrix $\mathbf{F}$ with the channel gain matrix $\mathbf{H}$ should yield a diagonal matrix to mitigate the effects of interference from other users:

$$\mathbf{HF} = \mathrm{diag}\left(\boldsymbol{\gamma}\right), \tag{8}$$

where the $\mathrm{diag}\left(\boldsymbol{\gamma}\right)$ is a diagonal matrix whose diagonal elements represent the corresponding symbol gains, γ_k. To satisfy that condition, the ZF beamforming matrix $\mathbf{F}$ is:

$$\mathbf{F} = \mathbf{H}^T\left(\mathbf{H}\mathbf{H}^T\right)^{-1}\mathrm{diag}\left(\boldsymbol{\gamma}\right). \tag{9}$$

When the objective function is considered as maximization of the total SE and a perfect channel knowledge at the receiver side is assumed, the optimization problem according to the given constraints is formulated as:

$$\begin{aligned} \underset{\gamma_k}{\text{maximize}} \quad & \sum_{k=1}^{K}\log_2\left(1 + \frac{\eta\gamma_k}{\sigma_{n_k}^2}\right) \\ \text{subject to} \quad & |\mathbf{F}|\boldsymbol{\gamma} <= \mathbf{P} \\ & \frac{\eta\gamma_k}{\sigma_{n_k}^2} >= \mathbf{0} \end{aligned} \tag{10}$$

where η is the coefficient for the instantaneous BER target BER_T and equals to $\sqrt{-\left(\log\left(5BER_T\right)\right)^{-1}}$ according to [8]; and $\frac{\gamma_k}{\sigma_{n_k}^2}$ is the achieved signal-to-noise ratio (SNR) at the user k.

B. Channel Model

Calculation of the channel DC gain between the transmitter and users is divided into two parts [13]. The first part is the direct path gain between the transmitter and receiver, which is

ISBN 978-3-8007-3976-9

termed line of sight (LOS), and the second is the reflected path, non-line of sight (NLOS), from the transmitter to a reflection point and then to the receiver. The reflected paths are generally referred from wall to the receiver path. Thus, for the total channel DC gain calculation, side walls, ceiling and floor are considered as a reflection point in (11):

$$\mathbf{H} = H_{LOS} + \sum_{w=1}^{W} H_{NLOS,w}, \tag{11}$$

where W is equal to 6 (4 side walls, ceiling and floor), and H_{LOS} is:

$$H_{LOS} = \frac{(m+1)A_{R_x}G}{2\pi d^2_{T_x \to R_x}} \cos^m(\varphi_{T_x \to R_x}) \cos(\theta_{T_x \to R_x}) \text{rect}\left(\frac{\theta_{T_x \to R_x}}{FOV_{R_x}}\right), \tag{12}$$

where m is the Lambertian order and depends on the transmitter semi-angle, $\Psi_{\frac{1}{2},T_x}$, $(m = -\ln 2/\ln(\cos(\Psi_{\frac{1}{2},T_x})))$; G is the optical filter gain; A_{R_x} is the area of the receiver; φ is the divergence angle and θ is the incidence angle. The symbol $A \to B$ indexes the angles from A to B. FOV_{R_x} is the FOV of the receiver and the function $rect$ gives 0 or 1 according to ratio of the incidence angle and FOV of the receiver. If the absolute value of the ratio is smaller than or equal to 1, the $rect$ function gives 1 and otherwise, it gives 0.

Calculation of the NLOS path is also divided into two parts: transmission from the transmitter to a reflection point and the reflection point to the receiver, as given in (13). For the calculation of the reflected paths, each reflection surface (walls) is divided into sub-areas. Firstly, LOS transmission from transmitter to these sub-areas is calculated (14). When the sub-areas reflect the emitted light from the transmitter, they also act as a transmitter but the re-emitted light is degraded by a reflection coefficient, ρ, of the surface (15):

$$H_{NLOS,w} = \sum_{n_w=1}^{N_w} H_{T_x \to n_w} H_{n_w \to R_x} \tag{13}$$

$$H_{T_x \to n_w} = \frac{(m+1)\Delta A_{n_w}}{2\pi d^2_{T_x \to n_w}} \cos^m(\varphi_{T_x \to n_w}) \cos(\theta_{T_x \to n_w}) \text{rect}\left(\frac{\theta_{T_x \to n_w}}{FOV_{n_w}}\right) \tag{14}$$

$$H_{n_w \to R_x} = \frac{\rho_w (n+1) A_{R_x} G}{2\pi d^2_{n_w \to R_x}} \cos^n(\varphi_{n_w \to R_x}) \cos(\theta_{n_w \to R_x}) \text{rect}\left(\frac{\theta_{n_w \to R_x}}{FOV_{R_x}}\right) \tag{15}$$

In equation (14), ΔA_{n_w} is the area of the sub-area, and in the equation (15), n is the Lambertian order of the reflection surface. In general, n is accepted as 1.

C. Receiver

At the receiver side, as noted, the channel matrix $\mathbf{H}$ is assumed as perfectly known. Thus, the addition of DC bias can be removed easily:

$$\mathbf{r} = \mathbf{y} - \mathbf{HP}. \tag{16}$$

After the DC bias is removed, the received symbol for each user, r_k is decoded by maximum likelihood (ML) decoder:

$$\hat{s_k} = \arg\min_{\hat{s} \in S_k} \|r_k - \mathbf{H}_k \mathbf{F}_k \hat{s}\|^2 \tag{17}$$

where $\hat{s_k}$ is the decoded data for user k; S_k is the set of all possible values of the 2-PAM shaping signals $\hat{s}$; and $\mathbf{H}_k$ and $\mathbf{F}_k$ are the channel DC gain and precoder vectors for user k, respectively.

TABLE I. SIMULATION PARAMETERS

Transmitter Parameters	**Value**
Number of LED arrays, N_t	1
Number of LEDs in a LED array, L	16
Outer Circle Radius, R_o	42.5 mm
Inner Circle Radius, R_i	21.25 mm
LED Semi-Angle, $\Psi_{\frac{1}{2},T_x}$	30°, 45°,60°
LED Bias Power - Upper Limit, $P_{b,up}$	20 dBm
LED Bias Power - Lower Limit, $P_{b,low}$	-40 dBm
Receiver Parameters	**Value**
Number of PDs at each user, N_r	1
PD Responsivity, r	0.4 A/W
PD Field-of-View, FOV_{R_x}	30°, 45°,60°
PD Physical Area, A_{R_x}	1 cm^2
Optical Filter Gain, G	1
System Geometry Parameters	**Value**
Transmitter Height	3 m
Receiver Height	0.75 m
Room Dimensions - Length x Width x Height	4 x 4 x 3 m
Reflection Coefficient - Side Wall, ρ_{wall}	0.9
Reflection Coefficient - Floor, ρ_{floor}	0.2
Reflection Coefficient - Ceiling, $\rho_{ceiling}$	0.8
Wall Division Area, ΔA_{n_w}	25 cm^2
System Parameters	**Value**
Bandwidth, B	50 MHz
Number of Users	4, 6, 8, 10
Pre-Amplifier Noise Density, i_{amp}	5x10^{-12} A/Hz$^{-1/2}$
Ambient Light Photocurrent, χ_{amp}	10.93 A/m^2/Sr
Bit Error Rate Target, BER_T	10^{-3}

III. SYSTEM SIMULATION

In this section, firstly the transmitter structure used in all simulations is introduced. To solve the optimization problem given in equation (10), the CVX optimization software tool is used [14]. Also, the channel power distribution of the given transmitter structure is presented for different semi-angles. Then, the simulation scenarios considered in this study are described. Next, all of the parameters used in the simulations are given, and finally the average BER and total SE results are presented.

A. Simulation Parameters

The system parameters used within the simulations are given in Table I. The optical filter gain G is assumed to be 1 and system bandwidth B is assumed to be 50 MHz in all of the simulations. Also, the receiver is assumed to point upwards and all LEDs are biased with the same DC power P_b in all simulations.

B. Transmitter Structure

Existing light fixtures consist of a different number of LEDs according to manufacturer design. In this study, an LED array consisting of 16 LEDs $(L = 16)$ is considered. As shown in Fig. 1, the LED array used has 10 LEDs on an outside circle, 5 LEDs on an inner circle and 1 LED at the center of the circle; all LEDs point downwards. Fig. 2 shows channel power distribution on the receiver height plane for different semi-angle values when the given LED array is used. Inherently, a small semi-angle value has more direct propagation along its orientation. Thus, variation of the channel power between the edge and center of the room becomes smaller by using LEDs with large semi-angle degrees.

C. Simulation Scenarios

To investigate the effects of the transceiver parameters, three different scenarios are considered in the system level

ISBN 978-3-8007-3976-9

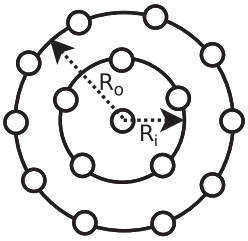

Fig. 1. LED array structure

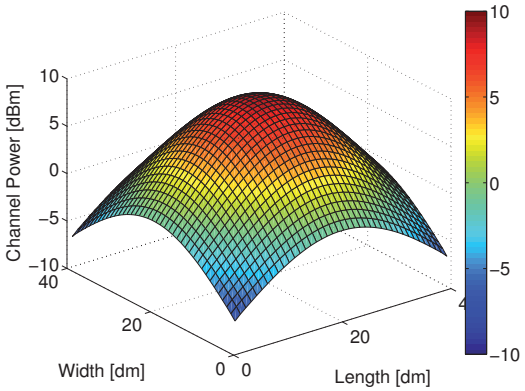

(a) $\Psi_{\frac{1}{2},T_x} = 30^o$

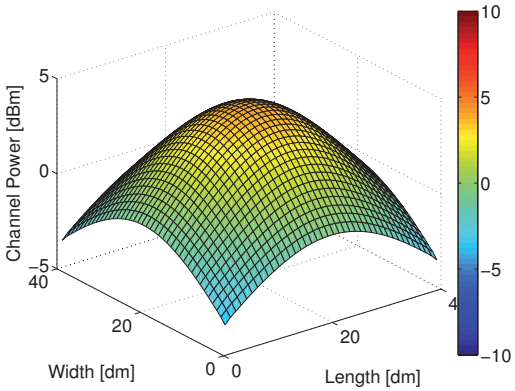

(b) $\Psi_{\frac{1}{2},T_x} = 60^o$

Fig. 2. Channel power distribution along the room

simulations. The location of the users according to the first two scenarios considered is given in Table II. In the first two scenarios, the generated channel DC gains are symmetrical due to the location of the users where 4 users are deployed in both scenarios. This symmetry is discounted in scenario 3, and several number of users are located randomly inside the room. In all of the scenarios, the transmitter is located at the center of the room.

D. Simulation Results

The performance of the average BER and total SE is assessed by varying the transmitter semi-angle and the receiver FOV for the considered scenarios. In the first two scenarios, the performance of the system is obtained after 10^6 data

TABLE II. CONSIDERED SCENARIOS

Scenario	User 1	User 2	User 3	User 4
1	[1.00 1.00 0.75]	[1.00 3.00 0.75]	[3.00 1.00 0.75]	[3.00 3.00 0.75]
2	[1.75 1.75 0.75]	[1.75 2.25 0.75]	[2.25 1.75 0.75]	[2.25 2.25 0.75]

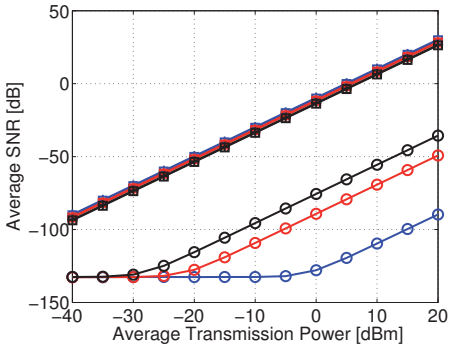

(a) Scenario 1

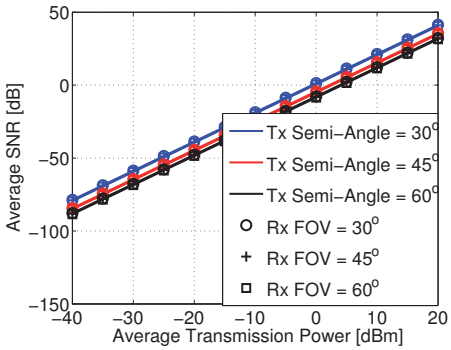

(b) Scenario 2

Fig. 3. Average SNR performance

transmissions. In the scenario 3, 10^6 data transmissions are used for 100 randomly generated positions to obtain the average BER and total SE. It is important to note that BER_T is assumed 10^{-3} and in some cases, bit error is not observed after some average transmission power values. This means error free communication is established after that average power value.

Fig. 3(a) and Fig. 3(b) show the average SNR performance of scenario 1 and scenario 2, respectively. In both scenarios 1 and 2, decreasing the semi-angle of the transmitter slightly decreases the average SNR performance of the given system. This trend can be explained when the channel power distributions in Fig. 2 and location of users in Table II are considered. The small transmitter semi-angles have larger power distribution along the room. Therefore SNR increases at the receiver side. In scenario 1, the distance between users and transmitter is greater than the scenario 2. Thus, a narrow receiver FOV degrades the achieved signal power level at the receiver according to (12) and (15).

In Fig. 4(a) and Fig. 4(b), the average BER performance of the first two scenarios is given. The first observation from the results for scenario 1 is that 30^o FOV at the receiver has the worst BER performance regardless of the transmitter semi-angle used. Also, when the transmitter has a small semi-angle value, the BER performance is outperformed, as shown in Fig. 4(a). However, Fig. 4(b) shows 30^o FOV has the best

ISBN 978-3-8007-3976-9

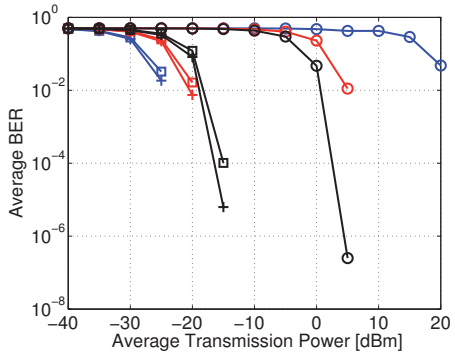

(a) Scenario 1

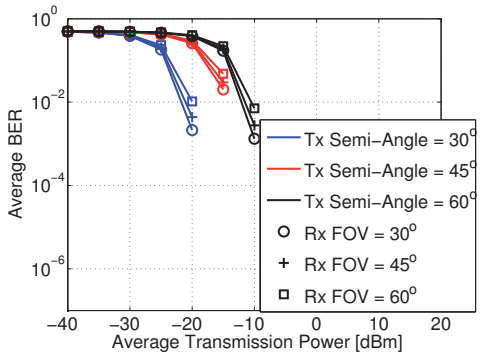

(b) Scenario 2

Fig. 4. Average BER performance

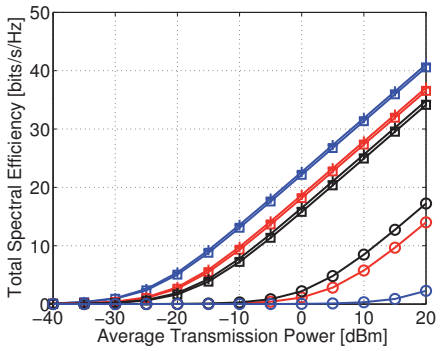

(a) Scenario 1

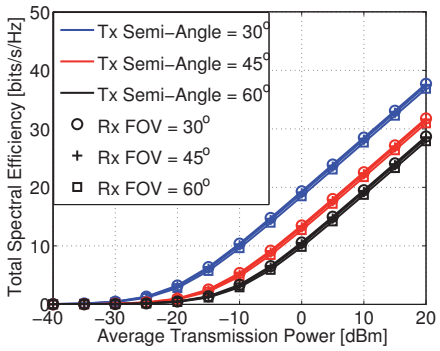

(b) Scenario 2

Fig. 5. Total SE performance

performance of all the used FOV degrees in the scenario 2.

The same explanation can be given for the effects of the receiver FOV and the transmitter semi-angle in the average BER performance results for the total SE performance. Fig. 5(a) shows the achieved total SE when the scenario 1 is considered. The system with 45^{o} and 60^{o} FOV at the receiver has 41 bits/s/Hz, 37 bits/s/Hz and 34 bits/s/Hz total SE when the transmitter semi-angles are 30^{o}, 45^{o} and 60^{o}, respectively. However, when the receiver has 30^{o} FOV, the total SE performance is 3 bits/s/Hz, 15 bits/s/Hz and 17 bits/s/Hz for the transmitter semi-angles 30^{o}, 45^{o} and 60^{o}, respectively. Although a wide transmitter semi-angle has a low channel power distribution, the performance degradation of the narrow receiver FOV degrees are compensated by using wide semi-angles.

Furthermore, in scenario 1, after -25 dBm, -20 dBm and -10 dBm average transmission power, the total SE of the system with 45^{o} and 60^{o} receiver FOV increases linearly with the increased transmission power when the transmitter semi-angles are 30^{o}, 45^{o} and 60^{o}, respectively. However, this power level is 5 dBm greater for all of the semi-angles used in scenario 2. When the users are located close to the transmitter, scenario 2, the receiver FOV degree does not have a significant effect on the total SE performance, as shown in Fig. 5(b). Nonetheless, the total SE performance decreased approximately 4 bits/s/Hz for all of the semi-angles used in scenario 2.

In addition, the average BER and total SE performance of the randomly distributed multiple users is investigated in scenario 3. Firstly, the transmitter with 30^{o} semi-angle is performed by varying the receiver FOV and number of randomly deployed users. Fig. 6(a) shows when 4 and 6 users are deployed in the system, the BER_T is achieved for the 45^{o} and 60^{o} receiver FOV angles within the used average transmission power levels. Also, the receiver with 45^{o} FOV achieves BER_T when the system has 8 users. Additionally, the performance of the receiver with FOV of 60^{o} dramatically decreased when the number of deployed users is increased. The total SE performance of the transmitter with 30^{o} semi-angle is shown in Fig. 6(b). The receiver with 45^{o} FOV has better SE performance than with 30^{o} and 60^{o} FOV. The maximum achieved total SE is 50 bits/s/Hz when the receiver has 45^{o} FOV and the system has 6, 8 and 10 users.

Secondly, the 60^{o} transmitter semi-angle is used in scenario 3. Fig. 7(a) shows the average BER performance of a various number of users and receiver FOV degrees. The 45^{o} and 30^{o} FOV at the receiver achieved the BER_T when 4, 6 and 8 users are deployed, whereas the receiver with 60^{o} FOV achieved the targeted BER only for 4 and 6 users. The total SE performance of the 60^{o} semi-angle is shown in Fig. 7(b). The performance of 60^{o} FOV in deployments with 8 and 10 users decreased but all other deployments with more than 4 users in the 60^{o} transmitter semi-angle outperformed the 30^{o} semi-angle performance.

IV. Conclusions

An investigation of the effects of transceiver physical features on the VLC system performance for a multi-user

ISBN 978-3-8007-3976-9

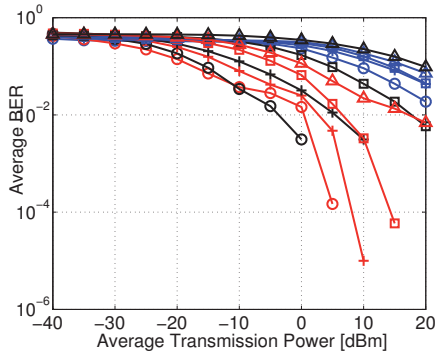

(a) Average BER

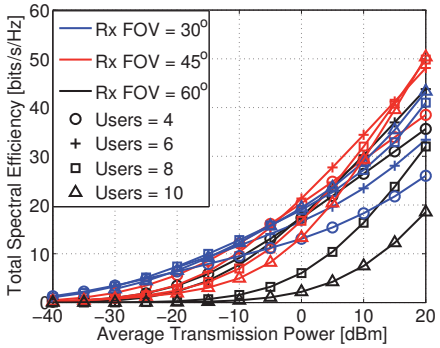

(b) Total SE

Fig. 6. Scenario 3 - Tx semi-angle = 30°

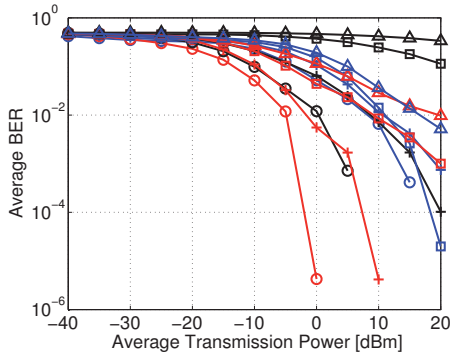

(a) Average BER

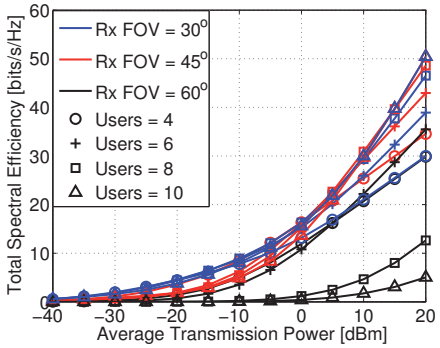

(b) Total SE

Fig. 7. Scenario 3 - Tx semi-angle = 60°

scenario using precoding at pre-transmission stage is reported. The simulation results indicate that the receiver with 45° FOV is feasible for a multi-user deployment when a single-cell LED array with multiple LEDs is considered. The semi-angle of the transmitter changes the channel power distribution within the room, inherently. Thus, the transmitter with a wide semi-angle is more appropriate for a multiple user system due to the random location of users. In addition, the designed precoder achieves the targeted BER when the maximum 8 users are deployed in the system within the given transmitter structure.

ACKNOWLEDGEMENT

Professor Haas acknowledges support from the Engineering and Physical Sciences Research Council (EPSRC) under the Established Career Fellowship grant EP/K008757/1 and Professor Panayirci acknowledges support from the COST-TUBITAK under the Research grant 113E307.

REFERENCES

[1] Cisco, "Cisco Visual Networking Index: Global Mobile Data Traffic Forecast Update, 2013-2018," Cisco White Paper, Tech. Rep., 2014.

[2] D. Tsonev, S. Videv, and H. Haas, "Light Fidelity (Li-Fi): towards all-optical networking," *Proc. SPIE*, vol. 9007, pp. 900 702–900 702–10, December 2013.

[3] H. Burchardt, N. Serafimovski, D. Tsonev, S. Videv, and H. Haas, "VLC: Beyond Point-to-Point Communication," *IEEE Commun. Mag.*, vol. 52, no. 7, pp. 98–105, July 2014.

[4] C.-X. Wang, F. Haider, X. Gao, X.-H. You, Y. Yang, D. Yuan, H. Aggoune, H. Haas, S. Fletcher, and E. Hepsaydir, "Cellular Architecture and Key Technologies for 5G Wireless Communication Networks," *IEEE Commun. Mag.*, vol. 52, no. 2, pp. 122–130, February 2014.

[5] L. Zeng, D. O'brien, H. Minh, G. Faulkner, K. Lee, D. Jung, Y. Oh, and E. T. Won, "High Data Rate Multiple Input Multiple Output (MIMO) Optical Wireless Communications Using White Led Lighting," *IEEE J. Select. Areas Commun.*, vol. 27, no. 9, pp. 1654–1662, December 2009.

[6] T. Fath and H. Haas, "Performance Comparison of MIMO Techniques for Optical Wireless Communications in Indoor Environments," *IEEE Trans. Commun.*, vol. 61, no. 2, pp. 733–742, February 2013.

[7] L. Wu, Z. Zhang, and H. Liu, "Modulation Scheme Based on Precoder Matrix for MIMO Optical Wireless Communication Systems," *IEEE Commun. Lett.*, vol. 16, no. 9, pp. 1516–1519, September 2012.

[8] K.-H. Park, Y.-C. Ko, and M. Alouini, "On the Power and Offset Allocation for Rate Adaptation of Spatial Multiplexing in Optical Wireless MIMO Channels," *IEEE Trans. Commun.*, vol. 61, no. 4, pp. 1535–1543, April 2013.

[9] Z. Yu, R. Baxley, and G. Zhou, "Multi-User MISO Broadcasting for Indoor Visible Light Communication," *IEEE International Conference on Acoustics, Speech, and Signal Processing (ICASSP)*, pp. 4849–4853, May 2013.

[10] H. Ma, L. Lampe, and S. Hranilovic, "Robust MMSE Linear Precoding for Visible Light Communication Broadcasting Systems," *IEEE Globecom Workshops*, pp. 1081–1086, Dec 2013.

[11] J. Lee and N. Jindal, "High SNR Analysis for MIMO Broadcast Channels: Dirty Paper Coding versus Linear Precoding," *IEEE Trans. Inform. Theory*, vol. 53, no. 12, pp. 4787–4792, Dec 2007.

[12] M. Joham, W. Utschick, and J. Nossek, "Linear Transmit Processing in MIMO Communications Systems," *IEEE Trans. Signal Processing*, vol. 53, no. 8, pp. 2700–2712, Aug 2005.

[13] J. Barry, J. Kahn, W. Krause, E. Lee, and D. Messerschmitt, "Simulation of Multipath Impulse Response for Indoor Wireless Optical Channels," *IEEE J. Select. Areas Commun.*, vol. 11, no. 3, pp. 367–379, Apr 1993.

[14] M. Grant and S. Boyd, "CVX: Matlab Software for Disciplined Convex Programming, Version 2.1," http://cvxr.com/cvx, Mar. 2014.

